



TiO₂ nanofibers of different crystal phases for transesterification of alcohols with dimethyl carbonate

Xingguang Zhang, Xuebin Ke*, Zhanfeng Zheng, Hongwei Liu, Huaiyong Zhu*

School of Chemistry, Physics, and Mechanical Engineering, Queensland University of Technology, GPO Box 2434, Brisbane, Qld 4001, Australia

ARTICLE INFO

Article history:

Received 5 November 2013

Received in revised form

10 December 2013

Accepted 18 December 2013

Available online 27 December 2013

Keywords:

TiO₂ nanofibers

Transesterification

Apparent activation energy

Isotope labeling

ABSTRACT

TiO₂ nanofibers with different crystal phases have been discovered to be efficient catalysts for the transesterification of alcohols with dimethyl carbonate to produce corresponding methyl carbonates. Advantages of this catalytic system include excellent selectivity (>99%), general suitability to alcohols, reusability and ease of preparation and separation of fibrous catalysts. Activities of TiO₂ catalysts were found to correlate with their crystal phases which results in different adsorption abilities and activation energies on the catalyst surfaces. The kinetic isotope effect (KIE) investigation identified the rate-determining step, and the isotope labeling of oxygen-18 of benzyl alcohol clearly demonstrated the reaction pathway. Finally, the transesterification mechanism of alcohols with dimethyl carbonate catalyzed by TiO₂ nanofibers was proposed, in which the alcohol released the proton to form benzyl alcoholic anion, and subsequently the anion attacked the carbonyl carbon of dimethyl carbonate to produce the target product of benzyl methyl carbonate.

© 2013 Elsevier B.V. All rights reserved.

1. Introduction

Methylation, carbonylation, carboxylation, and transesterification are important organic reactions and are extensively applied in industry for producing fine chemicals [1,2]. Conventional processes, for instance, the conversion of alcohols to methyl ethers or methyl carbonates [3,4], heavily depend on the classical base-promoted processes that involve toxic, hazardous, or corrosive compounds, such as alkyl halides, dimethylsulfate and phosgene, and consume over-stoichiometric amounts of strong bases [5,6]. Though efficient, these processes have raised severe concerns on safety and environments.

To address these problems, heterogeneous catalysts have been developed. For example, NaX [7], NaY [8], K₂CO₃ [9] and Al₂O₃ [10] are studied, using dialkylcarbonates (ROC(=O)OR), especially the environmentally benign reagent of dimethyl carbonate (DMC), as innovative alkylation agents in recent years [11]. DMC is a nontoxic and safe compound and shows unprecedentedly high selectivity (>99%) in the mono-methylation or carboxylation of aromatic alcohols, mercaptophenols, mercaptobenzoic acids, oximes, and amines [3,12]. However, more work needs to be done to explore new heterogeneous catalytic materials and to investigate the catalytic mechanism that is still ambiguous in terms of the rate-determining step and the cleavage of chemical bonds of reactants.

The carboxymethylation of bisphenol A with DMC catalyzed by TiO₂/SBA-15 has been reported [13]. It is stated that the species of Si–O–Ti bonds are active sites and that the interaction mode between Si–O–Ti and DMC plays a critical role in determining the selectivity. This work inspires us to explore whether TiO₂ can catalyze the transesterification of alcohols with dimethyl carbonate, considering the recent discoveries that metal oxides can interact with alcohols to form surface complexes and contribute to efficient catalysis [14–16]. The TiO₂ surface structures have been widely studied as photocatalysts, [17,18] demonstrating that different crystal phases have different photocatalytic consequences [19]. Primarily, TiO₂ exists in nature in four polymorphs: anatase (tetragonal, space group *I*4₁/*amd*), rutile (tetragonal, space group *P*4₂/*mnm*), brookite (orthorhombic, space group *Pbca*), and TiO₂(B) (monoclinic, space group *C*₂/*m*) [20,21]. If TiO₂ nanofibers can catalyze the transesterification, different crystal phases should exhibit different activities or selectivity, and thus the activation energies on each phase should vary. However these issues have not been clarified in reported studies.

In this study, TiO₂ nanofibers were employed to catalyze the transesterification of alcohols with DMC. Fibrous catalysts have some advantages compared with particles: (i) TiO₂ nanofibers have a higher aspect ratio with thickness of 40–100 nm and length up to 30 μm; therefore, they are easy to be recovered and reused from liquid reaction systems by filtration or sedimentation. (ii) The fibrous morphology efficiently alleviates the serious agglomerations usually existing in nanoparticles. [22,23] The catalysts were anatase (A), TiO₂(B), rutile (R), mixed anatase and TiO₂(B) – TiO₂(A + B),

* Corresponding authors. Fax: +61 07 31381804.

E-mail addresses: x.ke@qut.edu.au (X. Ke), hy.zhu@qut.edu.au (H. Zhu).

mixed anatase and rutile – $\text{TiO}_2(\text{A} + \text{R})$, commercial anatase and P_{25} particles (for control experiments). The scope of alcohols encompassed aromatic alcohols and alkyl alcohols, which indicated that TiO_2 catalysts possessed a general suitability to alcohols in the transesterification. Significantly, high activity and selectivity were achieved. The distribution of products was influenced by the phase compositions, and the catalytic activities also substantially depended on crystal phases of TiO_2 catalysts owing to their different abilities to adsorb reactants and different activation energies required to initiate the reactions. The activation energies of the transesterification on $\text{TiO}_2(\text{A})$, $\text{TiO}_2(\text{B})$, and $\text{TiO}_2(\text{R})$ were obtained by the kinetic study, and the rate-determining step was identified by the kinetic isotope effect (KIE) investigation. These findings, particularly the high selectivity on $\text{TiO}_2(\text{B})$, are promising because the methylcarbonate-ended chemicals are very active reagents for producing high molecular weight polymers, such as polycarbonates in the post-polycondensation step [24].

2. Experimental

2.1. Preparation of catalysts

All chemicals and commercial anatase and P_{25} were purchased from Sigma–Aldrich and were used without further treatment. Hydrogen-form titanate nanofibers ($\text{H}_2\text{Ti}_3\text{O}_7$) were prepared according to Ref 22. TiO_2 catalysts of different phases were obtained by calcining $\text{H}_2\text{Ti}_3\text{O}_7$ at different temperatures for 3 h with the step of increasing temperature of $5^\circ\text{C}/\text{min}$: $\text{TiO}_2(\text{B})$ (450°C , B phase of TiO_2), $\text{TiO}_2(\text{A} + \text{B})$ (550°C , uniform mixture of $\text{TiO}_2(\text{A})$ and $\text{TiO}_2(\text{B})$ in one nanofiber, not a mechanical mixture), $\text{TiO}_2(\text{A})$ (700°C , anatase), $\text{TiO}_2(\text{A} + \text{R})$ (850°C , uniform mixture of $\text{TiO}_2(\text{A})$ and $\text{TiO}_2(\text{R})$), $\text{TiO}_2(\text{R})$ (950°C , rutile). After treatment, all materials maintained nanofibrous morphology (see SEM images in Supplementary data, Section 1).

2.2. Characterizations

X-ray diffraction (XRD) patterns of the samples were recorded on a Philips PANalytical X'Pert PRO diffractometer using $\text{Cu K}\alpha$ radiation ($\lambda = 1.5418 \text{ \AA}$) operating at 40 kV and 40 mA with a fixed slit. The transmission electron microscopy (TEM) study on TiO_2 nanofibers was performed on the instrument of Philips CM200 TEM with the accelerating voltage being 200 kV, and high-resolution TEM (HR-TEM) study was carried out on a FEI Tecnai F20 operating at 200 kV. Diffuse reflectance UV/visible (DR-UV/vis) spectra were recorded on the Cary 5000 UV/vis–Nir Spectrophotometer to investigate the light absorption and emission behaviour of the samples. The measurement of IES (Infrared Emission Spectroscopy) was conducted on a Digilab FTS-60A spectrometer equipped with a TGS detector, and the instrument was modified by replacing the IR source with an emission cell. Identical amounts (in volume) of samples of TiO_2 with different crystal phases were loaded on the sample holder to form a uniform thin layer. During the measurement, the specimen was heated from 100°C to 450°C with the interval of 50°C in the flow of N_2 ($15 \text{ cm}^3/\text{min}$ controlled by a flow meter) in a closed but not sealed chamber for removing desorbed species from the sample. The interval between the two scans, for instance, between 100°C and 150°C , was two minutes for the sample to stabilize and reach temperature equilibrium. When the specimen was heated, the species adsorbed on the TiO_2 surface, such as adsorbed water and benzyl alcohol, were gradually removed. The extent of the removal depended on the adsorption strength of the species on the TiO_2 surface. The maximum temperature was 450°C to prevent the specimen from undergoing a phase change. By comparing the loss of adsorbed surface organic species during the heating process,

the adsorption ability of TiO_2 surfaces could be determined because the TiO_2 samples that had weaker adsorption ability lost adsorbed surface complexes more easily. The IES spectra at a lower temperature had more noise owing to the low signal-to-noise ratio resulted from the difference between the sample and the detector.

2.3. Catalytic test

Typically, 0.1 g of TiO_2 catalysts were added into 30 mL DMC and 2.0 mmol benzyl alcohol in a two-necked 100 mL round-bottomed glass flask. The air in the flask was replaced with argon prior to reaction. Then the side mouth of the glass reactor from which samples were taken was sealed by a stopper and the main mouth was connected to a reflux. The reactor was kept at 100°C in an oil bath with a magnetic stirring bar. The specimens were collected after 8 h, and analyzed in a Gas Chromatography (HP6890 Prometheus, the HP-5 column) to measure the concentration change of benzyl alcohol and products. GC–MS (6890-5793 Pegasus, the HP-5 column) was also employed to determine and analyze the products. Quantification of the products was obtained from the peak area ratios of the reactant and corresponding products. The reaction rate was defined as follows: reaction rate = (moles of reagent converted)/(moles of total active sites \times reaction time).

2.4. Isotope labeling experiment

Oxygen-18 (^{18}O) isotope-labeled benzyl alcohol ($\text{PhCH}_2^{18}\text{OH}$) was prepared by following the Ref 25: 0.4 g sodium (Na) metal was added to 3.0 mL 98% H_2^{18}O (from Huayi Isotope Co.) in a 25-mL round-bottomed flask, and 2.0 mL benzyl chloride was added into the flask. Then the mixture was heated by an oil bath to 150°C and refluxed for 48 h with continuous stirring. The products were purified by distillation and the obtained $\text{PhCH}_2^{18}\text{OH}$ was used in the transesterification reaction with DMC on $\text{TiO}_2(\text{B})$ to investigate the kinetic isotope effect (KIE). In addition, the reaction between $\text{PhCH}_2^{18}\text{OH}$ with DMC was conducted in the same procedure as described above just by replacing normal benzyl alcohol with $\text{PhCH}_2^{18}\text{OH}$. The products were also detected and analyzed by GC and GC–MS.

3. Results and discussions

3.1. Catalytic performance

The conversion of benzyl alcohol was in this order: $\text{TiO}_2(\text{B}) > \text{TiO}_2(\text{A} + \text{B}) > \text{TiO}_2(\text{A}) > \text{Commercial anatase} > \text{P}_{25} > \text{TiO}_2(\text{A} + \text{R}) > \text{TiO}_2(\text{R})$, as shown in Table 1. Commercial anatase and P_{25} were tested in control experiments. Commercial anatase showed a slightly lower conversion than that of $\text{TiO}_2(\text{A})$, and P_{25} exhibited slightly higher activity than $\text{TiO}_2(\text{A} + \text{R})$ but poor selectivity. The conversion and selectivity were excellent at 100°C on $\text{TiO}_2(\text{B})$ and $\text{TiO}_2(\text{A} + \text{B})$, indicating that the product was predominantly benzyl methyl carbonate (BMC). The distribution of products was also influenced by the phase composition, generally, BMC was the dominant product on most catalysts, whereas dibenzyl ether (DBE) was the major product on $\text{TiO}_2(\text{R})$ and $\text{TiO}_2(\text{A} + \text{R})$.

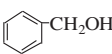
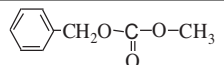
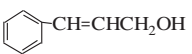

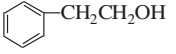
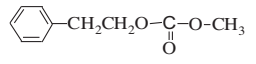
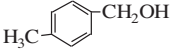
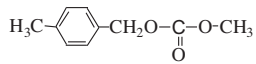
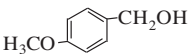
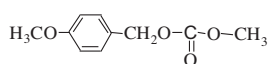
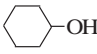
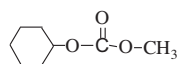
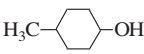
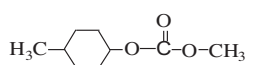
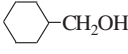
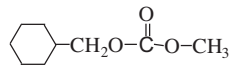
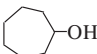
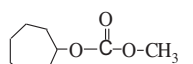
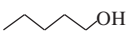
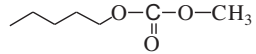
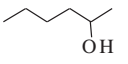
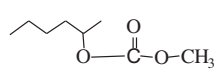
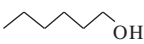
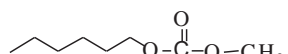
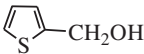
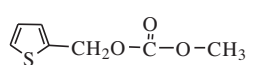
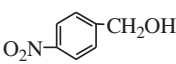
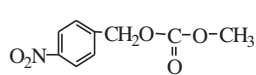
Table 2 showed the catalytic performance of $\text{TiO}_2(\text{B})$, which exhibited the best catalytic performance as shown in Table 1, for the transesterification of DMC with several sorts of alcohols to test its general applicability. The range of alcohols covers aromatic alcohols and alkyl alcohols, and most of alcohols reacted with DMC to give the corresponding methyl carbonates with a high activity and excellent selectivity. The conversions could be improved significantly if temperature was raised to 160°C (see Table S1 in Supplementary data, Section 2). These results demonstrated that

Table 1

The conversion and selectivity on different catalysts.

Catalyst	Conv. ^a (%)	Reaction rate [$10^{-3} \text{ mol g}^{-1} \text{ h}^{-1}$]	Select. ^b (%)			
			BME	BMC	DBE	DBC
TiO ₂ (A)	24.2	4.83		94.9	5.1	
TiO ₂ (B)	39.8	7.94		>99		
TiO ₂ (A + B)	37.8	7.54	6.3	93.7		
TiO ₂ (R)	6.7	1.34			>99	
TiO ₂ (A + R)	9.4	1.88			90.3	9.7
Commercial anatase (particles)	20.6	4.12	3.2	90.6	6.2	
Commercial P ₂₅ (particles)	10.7	2.14	1.9	14.4	76.5	7.2

^a Conversion of benzyl alcohol.^b BME represents benzyl methyl ether; BMC, benzyl methyl carbonate, DBE dibenzyl ether; and DBC, dibenzyl carbonate. Reaction conditions: DMC (30 mL), benzyl alcohol (2.0 mmol), catalyst (0.1 g), reaction time (8 h), temperature (100 °C), and argon atmosphere.**Table 2**Catalytic performances of TiO₂(B) for several alcohols.

Reagent	Preferred product	Conv. ^a (%)	Select. ^b (%)	Reaction rate [$10^{-3} \text{ mol g}^{-1} \text{ h}^{-1}$]
		39.8	>99	7.94
		18.6	47.5	3.71
		40.1	>99	8.01
		48.1	>99	9.61
		70.4	88.3	14.06
		44.9	>99	8.97
		37.9	91.1	7.57
		52.7	>99	10.52
		36.9	>99	7.37
		40.7	>99	8.12
		32.8	>99	6.55
		45.5	>99	9.09
		50.7	>99	10.13
		52.0	>99	10.39

^a Conversion of the reactant.^b Selectivity towards the preferred product. Reaction conditions: DMC (30 mL), alcohol (2.0 mmol), catalyst (0.1 g), reaction time (8 h), temperature (100 °C), and argon atmosphere.

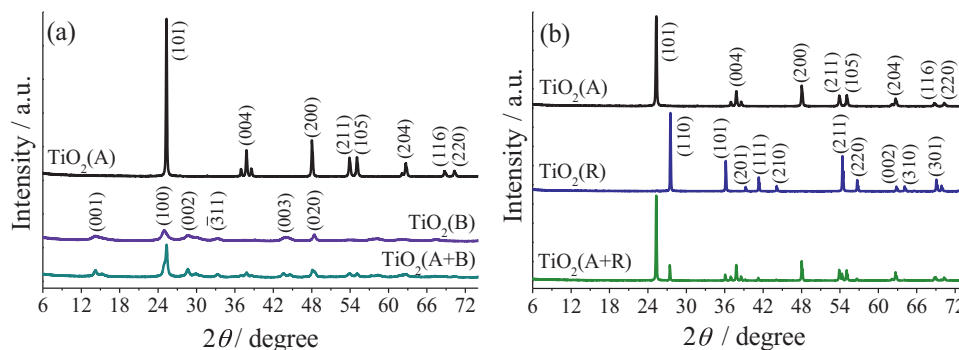


Fig. 1. (a) X-ray diffraction (XRD) patterns of TiO₂(A), TiO₂(B), and TiO₂(A + B). (b) XRD patterns of TiO₂(A), TiO₂(R), and TiO₂(A + R); ("A" refers to anatase, "B" refers to TiO₂(B) and "R" refers to rutile).

TiO₂ catalysts had universal applicability for the transesterification of alcohols with DMC.

3.2. XRD and TEM analyses of TiO₂ catalysts

Fig. 1(a) and (b) displays the XRD patterns of TiO₂ catalysts. The single-phase nanofiber of TiO₂(A), TiO₂(B), and TiO₂(R) all showed its characteristic diffraction peaks. Both TiO₂(A + B) and TiO₂(A + R) indicated a mixed phase structure. The molar ratio between TiO₂(B) and TiO₂(A) phase in TiO₂(A + B) was estimated from the intensity ratio ($I_{33.4}/I_{37.8} = 65.3\%$) of the peak at $2\theta = 33.4^\circ$ to the peak at $2\theta = 37.8^\circ$, which were reflections from the (3 1 1) plane of TiO₂(B) (JCPDS 74-1940) and the (0 0 4) plane of anatase (JCPDS 21-1272), respectively [22]. Similarly, the molar ratio between TiO₂(R) and TiO₂(A) in TiO₂(A + R) was calculated from the intensity ratio ($I_{27.5}/I_{25.3} = 34.5\%$) of the peak at $2\theta = 27.5^\circ$ to the peak at $2\theta = 25.3^\circ$, which were reflections from the (1 1 0) plane of TiO₂(R) and the (1 0 1) plane of TiO₂(A), respectively.

Detailed crystal phase information of TiO₂(A), TiO₂(B), and TiO₂(A + B) is confirmed by high-resolution TEM analyses as presented in Fig. 2 (and Raman spectra in the Supporting data, Section 3). Here we mainly focus on TiO₂(A) and TiO₂(B) because they performed much better than TiO₂(R) did in catalytic activities. The

electron diffraction pattern in Fig. 2(b) identifies only anatase single crystals; and Fig. 2(d) shows the fibers have merely TiO₂(B) single crystals. Furthermore, the selected area electron diffraction (SAED) analysis confirms the co-existence of both anatase and TiO₂(B) phases in the TiO₂(A + B) nanofibers, as shown in Fig. 2(e) that the dark anatase grain can be observed on the surface of TiO₂(B). The SAED analyses (Fig. 2(g)) show that two phases coexist in a state of intimate contact with each other and join tightly; no voids between the crystals of the two phases are observed. The TEM images and SEM pictures (Supplementary data, Section 1) confirm that these samples inherited the fibrous morphology of the parent hydrogen-form titanate nanofibers after calcinations.

3.3. Adsorption ability of TiO₂ catalysts

The ability of TiO₂ catalysts to adsorb reactants was investigated by UV/vis spectra and Infrared Emission Spectroscopy (IES). The samples were prepared by mixing 0.1 mL of benzyl alcohol or DMC and 0.1 g of TiO₂ catalysts together for 4 h at room temperature, followed by washing thoroughly and drying the specimens at 80 °C under vacuum conditions for 24 h. In doing this at the same conditions, the amount of residue adsorbates and the removal extents under thermal treatment should qualitatively reflect the

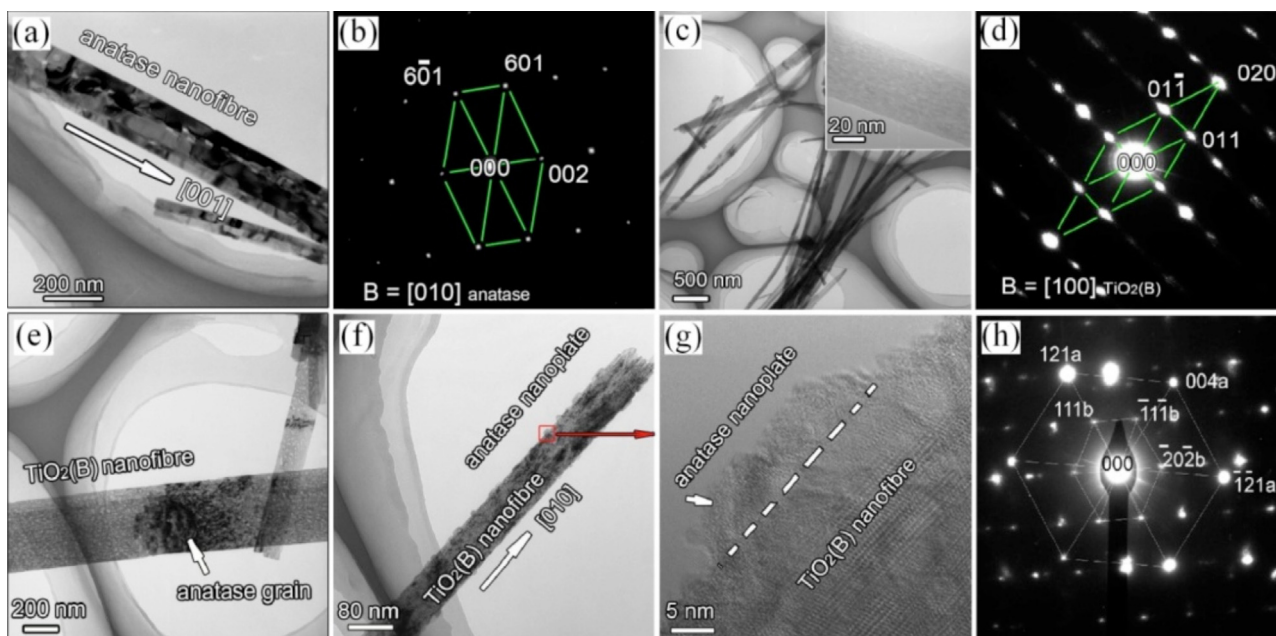


Fig. 2. High-resolution TEM images of (a) TiO₂(A) (anatase) nanofibers, (b) electron diffraction pattern of TiO₂(A), (c) TiO₂(B) nanofibers, (d) electron diffraction pattern of TiO₂(B), (e)–(g) TiO₂(A + B) nanofibers, and (h) electron diffraction pattern of TiO₂(A + B).

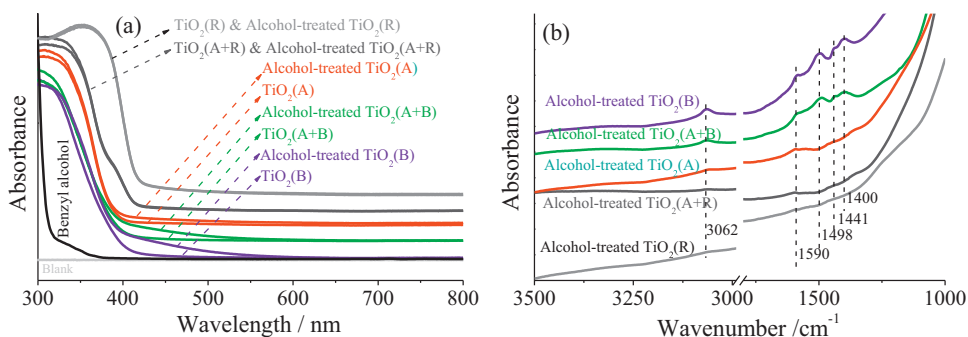


Fig. 3. (a) UV/vis spectra of benzyl alcohol, TiO₂ catalysts and benzyl alcohol-adsorbed TiO₂ catalysts (the “TiO₂(R) & DMC-treated TiO₂(R)” means that two curves of each were so similar that they overlapped); (b) IES spectra of benzyl alcohol-adsorbed TiO₂ catalysts collected at 400 °C.

adsorption ability of TiO₂ catalysts. The spectrum of pure benzyl alcohol and DMC were also collected for comparison.

The UV/vis spectra of benzyl alcohol, TiO₂ catalysts, and benzyl alcohol-adsorbed TiO₂ catalysts (Fig. 3(a)) showed that benzyl alcohol and TiO₂ catalysts exhibited no measurable absorption in the visible region (please note that the curves have been vertically moved upward to arrange neatly for clear comparison). As for the benzyl alcohol-adsorbed TiO₂ catalysts, TiO₂(B) and TiO₂(A+B) exhibited obvious absorption of visible light, TiO₂(A) showed slight absorption; whereas TiO₂(A+R) and TiO₂(R) almost had no absorption. These results demonstrated that TiO₂(B) and TiO₂(A+B) had stronger ability to adsorb benzyl alcohol than TiO₂(A+R) and TiO₂(R) did. In some studies, the interaction between benzyl alcohol and anatase is assigned to the TiO₂ surfaces interacting with the –CH₂OH group or the phenyl ring of benzyl alcohol [26,27].

To further determine the adsorption ability of TiO₂ catalysts, the IES spectra (Fig. 3(b)) of benzyl alcohol-adsorbed TiO₂ catalysts were collected at 400 °C. At this temperature, the crystal phase of TiO₂ catalysts remained unchanged, but partial organic species on the surface of some catalysts had been removed because of different adsorption abilities of TiO₂ catalysts. To be clear, the adsorbates may be not benzyl alcohol molecules at 400 °C but decomposed organic species, such as aromatic rings and benzyloxy/alkoxy groups that are surface complexes formed between alcohols and metal oxides [28]. Several peaks could be identified from the spectra. The peak centered at 3062 cm⁻¹ and 1440 cm⁻¹ were assigned to the C–H stretching vibration and the C–H in-plane bending vibration of the aromatic rings [27]. The band at 1590 cm⁻¹ indicated the C–C ring stretching vibration [29]. The band at 1498 cm⁻¹ could be readily ascribed to the skeletal vibration of the aromatic ring and the band centered at 1400 cm⁻¹ could be identified as the ring stretching mode [30]. From the extent of the removal of decomposed organic species, one can deduce the ability of TiO₂ catalysts to adsorb the organic species, because the interaction between them and TiO₂ catalysts originated from strong chemical adsorption after thoroughly washing and 24-h drying under the vacuum condition. The weaker adsorption results in losing adsorbed organic species more easily on such as TiO₂(R) which lost every peak of organic species at 400 °C, whereas TiO₂(B) still held some surface organic species. Therefore, it could be generally concluded that the adsorption ability of TiO₂ catalysts was in the following order: TiO₂(B) > TiO₂(A+B) > TiO₂(A) > TiO₂(A+R) > TiO₂(R), which corresponded excellently to the tendency as shown in the UV/vis spectra (Fig. 3(a)).

The UV/vis spectra of DMC, TiO₂ catalysts, and DMC-adsorbed TiO₂ catalysts showed that no obvious difference could be found in the spectra of each TiO₂ catalyst and its DMC-adsorbed counterpart (see Supplementary data, Section 4). Moreover, the

IR-ATR (Attenuated Total Reflectance) spectra of DMC, TiO₂(B) and DMC-adsorbed TiO₂(B) provided no convincing evidence that DMC was still adsorbed on the surface of TiO₂(B) after washing and 24-h drying under the vacuum condition. These results suggested that TiO₂ catalysts had extremely weak ability to adsorb DMC molecules.

3.4. Kinetic study

The difference in catalytic activities and the adsorption ability of TiO₂ catalysts inspire us that the activation energies on the TiO₂ catalysts should be different. Here TiO₂(B), TiO₂(A) and TiO₂(R) were used to investigate the activation energy of the reaction between benzyl alcohol and DMC at several temperatures: 40 °C, 60 °C, 80 °C and 100 °C. Samples were collected after different periods of reaction time within 8 h to calculate the conversion of benzyl alcohol (X_b), and a first-order dependence of the reaction rate on the concentration of benzyl alcohol was found. The plot of $-\ln(1 - X_b)$ versus the reaction time t created several straight lines (see Supplementary data, Section 5), according to the equation of the first-order reaction: $-\ln(1 - X_b) = kt$, in which k is the rate constant of the reaction. For each line, the slope is equal to the negative value of the rate constant k so that four values of k can be obtained at four different temperatures for each catalyst.

According to the Arrhenius equation, three straight lines of $\ln(k)$ versus $(1/T)$ can be obtained, corresponding to TiO₂(B), TiO₂(A) and TiO₂(R) as shown in Fig. 4, and the value of the slope equals to $-E_a/R$ (E_a means the apparent activation energy). Then the

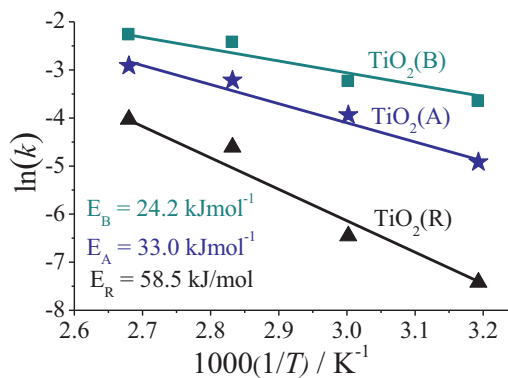
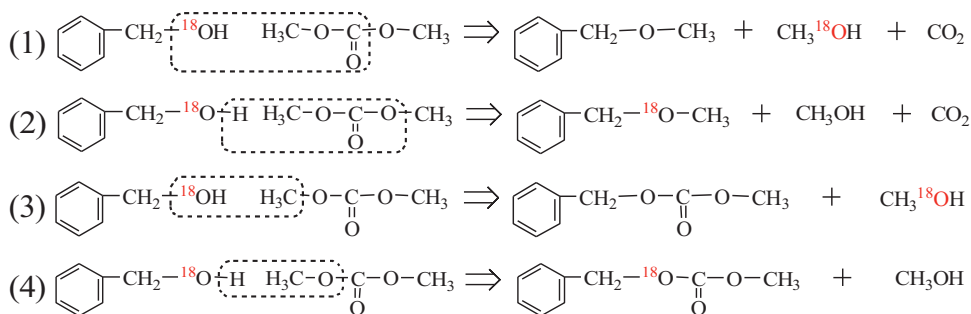


Fig. 4. The plot of $\ln(k)$ versus $(1/T)$ for deriving the apparent activation energy. Reaction conditions: DMC (30 mL), benzyl alcohol (2.0 mmol), catalyst (0.1 g), and argon atmosphere.



Scheme 1. Four possible reactions between benzyl alcohol and dimethyl carbonate.

activation energies on $\text{TiO}_2(\text{B})$ (denoted as E_B), $\text{TiO}_2(\text{A})$ (denoted as E_A), and $\text{TiO}_2(\text{R})$ (denoted as E_R) can be calculated, being 24.2 kJ mol^{-1} , 33.0 kJ mol^{-1} and 58.5 kJ mol^{-1} , respectively. These results again suggested that $\text{TiO}_2(\text{B})$ could activate the reaction between benzyl alcohol and DMC more easily than $\text{TiO}_2(\text{R})$ did.

3.5. Discussion on the difference in activities of TiO_2 catalysts

One may wonder why TiO_2 catalysts with different crystal structures exhibit different activities. First, the adsorption ability of TiO_2 catalysts should play a vital role in determining the catalytic activity because stronger adsorption ability facilitates the concentration of reactants from solvent. The UV/vis and IES spectra of benzyl alcohol-adsorbed TiO_2 catalysts have demonstrated that the order of adsorption ability matches excellently to the catalytic activities of the TiO_2 catalysts in the transesterification of benzyl alcohol with DMC. Second, the results of kinetic study suggested that the activation energy on $\text{TiO}_2(\text{B})$ was much lower than that on $\text{TiO}_2(\text{R})$, thus activating reactants more easily to initiate the transesterification. Third, the difference in the specific surface areas of TiO_2 catalysts should have a negligible influence on the catalytic activities because the Brunauer–Emmett–Teller (BET) surface areas of these TiO_2 catalysts in use are similar, ranging from 19.8 to $38.6 \text{ m}^2 \text{ g}^{-1}$ (see Table S2 in Supplementary data, Section 6). Fourth, the acidity of catalysts has been reported to affect the transesterification of alcohol and dimethyl carbonate over zeolites,[31] γ -alumina,[32] and metal-organic frameworks (MOFs)[33]. Recently, the acidity of different TiO_2 polymorphs has been investigated using IR spectroscopy of adsorbed pyridine, Zeta-potential measurements and catalytic activity in the model reaction of isopropanol decomposition [34]. It is found that $\text{TiO}_2(\text{R})$ presents a quite low acidity compared with $\text{TiO}_2(\text{A})$, and thus shows a poor activity in the decomposition of isopropanol. This result is consistent with our observation that $\text{TiO}_2(\text{R})$ had the weak adsorption ability, the high activation energy, and the low catalytic activity. In addition, both dehydration and transesterification are catalyzed by acidic sites and are competitive reactions in the system of benzyl alcohol and DMC. The crystal phase/facets, weak acid sites, and weak adsorption abilities of rutile may favour the dehydration rather than transesterification, as the primary product on $\text{TiO}_2(\text{R})$ and $\text{TiO}_2(\text{A}+\text{R})$ is dibenzyl ether instead of benzyl methyl carbonate (Table 1). On the basis of above analyses, it should be safe to conclude that the difference in catalytic activities of TiO_2 catalysts results from their different abilities to adsorb and activate reactants.

3.6. Investigation of $^{16}\text{O}/^{18}\text{O}$ kinetic isotope effect (KIE) and reaction pathway

The oxygen-18 isotope labeled benzyl alcohol ($\text{PhCH}_2^{18}\text{OH}$) was employed to identify which bond of benzyl alcohol or DMC broke,

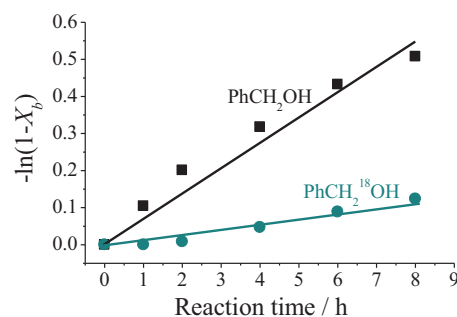


Fig. 5. Comparison between the transesterification of DMC with benzyl alcohol (PhCH_2OH) and ^{18}O -enriched benzyl alcohol ($\text{PhCH}_2^{18}\text{OH}$). The slopes of the lines correspond to the rate constants. Reaction conditions: DMC (30 mL), benzyl alcohol (2.0 mmol), catalyst (0.1 g), and reaction time (8 h), temperature (100°C), and argon atmosphere.

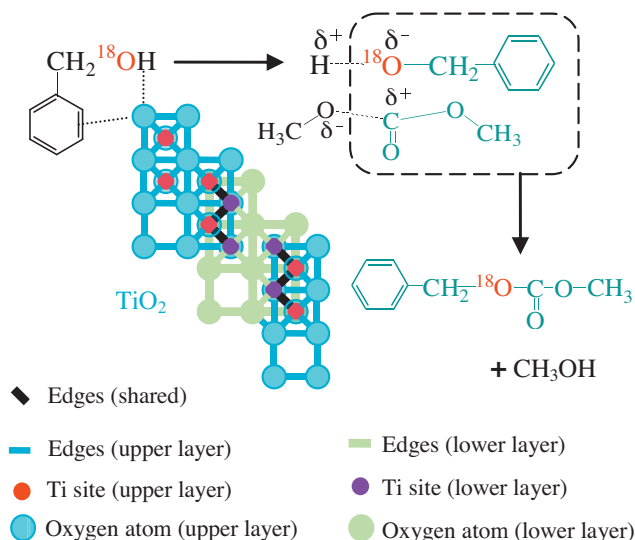
and whether the breakage of this bond determined the reaction rate (rate-determining step). The experiment was performed on $\text{TiO}_2(\text{B})$ at 100°C just as the experiment done for normal benzyl alcohol (PhCH_2OH). Samples were collected to calculate the conversions (X_b), and a linear relationship between $-\ln(1-X_b)$ and the reaction time t was obtained (see Fig. 5). The slope of the line corresponds to the rate constant k : for $\text{PhCH}_2^{18}\text{OH}$, $k_{18} = 3.79 \times 10^{-6} \text{ s}^{-1}$ and for $\text{PhCH}_2^{16}\text{OH}$, $k_{16} = 1.89 \times 10^{-5} \text{ s}^{-1}$. Thus $\text{KIE} = k_{16}/k_{18} = 4.99$, indicating that the bond breakage of $\text{C}-^{18}\text{O}$ or $^{18}\text{O}-\text{H}$ was the rate-determining step [25,35].

In the reaction between benzyl alcohol and DMC, four major reactions (Eqs. (1)–(4) as shown in Scheme 1) may occur, depending on the positions in which the chemical bonds break:

According to the analysis of GC–MS, only the product of ^{18}O -enriched benzyl methyl carbonate was detected when $\text{PhCH}_2^{18}\text{OH}$ was used (see more details in Supplementary data, Section 7). Therefore, Eqs. (1)–(3) could be ruled out, and the reaction path was Eq. (4). It became transparent that the bond cleavage was on $\text{O}-\text{H}$ in benzyl alcohol and on $\text{CH}_3\text{O}-\text{C}$ in DMC to produce the desired product of benzyl methyl carbonate.

3.7. Mechanistic study

In some studies, DMC conformers are observed on such as NaY and $\text{TiO}_2/\text{MCM-41}$ [8,36], showing that the electric-field-induced polarization of DMC molecules can lead to the activation (elongation and weakening) of the $\text{O}-\text{CH}_3$ and/or $\text{C}-\text{OCH}_3$ bonds. The activated DMC molecules can form both *cis-cis* and *cis-trans* species (conformers) to give carboxylated products ($<90^\circ\text{C}$) or methylated products ($>120^\circ\text{C}$) [3]. However, the results of the UV/vis and the IR-ATR spectra (see Supplementary data, Section 4) cannot verify



Scheme 2. Proposed mechanism on the transesterification of benzyl alcohol with dimethyl carbonate on $\text{TiO}_2(\text{B})$. The illustration of the structure of $\text{TiO}_2(\text{B})$ projected along the [0 1 0] direction [37].

a strong interaction between DMC and TiO_2 catalysts. Therefore, we tentatively speculate that the catalytic activity of TiO_2 catalysts stems from the direct activation of benzyl alcohol by TiO_2 catalysts, attended by reaction with DMC in the proximity of activated benzyl alcohol molecules. Moreover, the fact that merely carboxylated products were detected on $\text{TiO}_2(\text{B})$ at 160°C indicated that no other DMC conformers formed in the reactions (see Table S1 Supplementary data, Section 2).

On the basis of experimental results and relevant literature, a possible mechanism on the transesterification of benzyl alcohol with DMC on $\text{TiO}_2(\text{B})$ can be proposed as shown in Scheme 2. $\text{TiO}_2(\text{B})$ adsorbed benzyl alcohol molecules on the surfaces through the interaction with the $-\text{CH}_2\text{OH}$ group or the phenyl rings [26,27]. Then the adsorbed benzyl alcohol molecules were activated by $\text{TiO}_2(\text{B})$ and reacted with DMC. As demonstrated by the isotope labeling experiment that benzyl alcohol released its proton (H^+) from the hydroxyl group (rate-determining step) to produce the benzyl alcoholic anion (PhCH_2O^-), which attacked the carbonyl carbon of DMC to give the product of BMC. The released proton (H^+) reacted with the methoxy anion (CH_3O^-) to give methanol.

4. Conclusion

The transesterification of alcohols with dimethyl carbonate was discovered to successfully proceed on TiO_2 nanofibrous catalysts with different crystal phases. Several basic conclusions could be obtained on the grounds of experimental results.

Catalytic activities at 100°C were: $\text{TiO}_2(\text{B}) > \text{TiO}_2(\text{A} + \text{B}) > \text{TiO}_2(\text{A}) > \text{Commercial anatase} > \text{P}_{25} > \text{TiO}_2(\text{A} + \text{R}) > \text{TiO}_2(\text{R})$, and the selectivity on most catalysts was excellent (>99%). The difference in catalytic activities was demonstrated to correlate with the adsorption ability and the different activation energies on TiO_2 catalysts.

The KIE investigation and the mechanistic study by ^{18}O isotope labeling of benzyl alcohol substantially identified the rate-determining step and the reaction pathway, in which the O–H bond of benzyl alcohol cleaved to give the proton (H^+) and the benzyl alcoholic anion (PhCH_2O^-) that attacked the carbonyl carbon of DMC to produce the desired product of benzyl methyl carbonate.

Finally, the mechanism of TiO_2 -catalyzed transesterification was proposed, and the mechanism was partly different from that

occurs on zeolite or acid-base catalysts, because TiO_2 catalysts produced no methylated products even though the reaction temperature was higher than 120°C . Moreover, TiO_2 catalysts can also be repeatedly used while maintaining excellent catalytic activity (see Supplementary data, Section 8), and most significantly, we discover that TiO_2 -based catalysts offer a great promise in thermal-driven reactions instead of exclusively in photocatalytic reactions.

Supplementary information

Supplementary data associated with this article can be found in the online version, including Raman spectra of TiO_2 nanofibers of different crystal phases, SEM images of different phases of TiO_2 catalysts, UV/vis and IR spectra of DMC and TiO_2 , BET surface areas of TiO_2 catalysts, kinetic study, plots of $-\ln(1 - X_b)$ versus the reaction time, results of oxygen-18 labeled benzyl alcohol ($\text{PhCH}_2^{18}\text{OH}$), reusability of $\text{TiO}_2(\text{A})$ and $\text{TiO}_2(\text{B})$, the catalytic performance of $\text{TiO}_2(\text{B})$ for several alcohols at 160°C .

Acknowledgements

This research is supported by the Australian Research Council (ARC) and X. Ke is indebted to QUT and the Queensland State Government for a Smart Futures Fellowship.

Appendix A. Supplementary data

Supplementary material related to this article can be found, in the online version, at <http://dx.doi.org/10.1016/j.apcatb.2013.12.035>.

References

- [1] O. Ilgen, A.N. Akin, Appl. Catal. B 126 (2012) 342–346.
- [2] N. Boz, N. Degirmenbasi, D.M. Kalyon, Appl. Catal. B 89 (2009) 590–596.
- [3] P. Tundo, M. Selva, Acc. Chem. Res. 35 (2002) 706–716.
- [4] B. Xu, R.J. Madix, C.M. Friend, J. Am. Chem. Soc. 133 (2011) 20378–20383.
- [5] A.-A.G. Shaik, S. Sivaram, Chem. Rev. 96 (1996) 951–976.
- [6] P. Anastas, N. Eghbali, Chem. Soc. Rev. 39 (2010) 301–312.
- [7] M. Selva, E. Militello, M. Fabris, Green Chem. 10 (2008) 73–79.
- [8] F. Bonino, A. Damin, S. Bordiga, M. Selva, P. Tundo, A. Zecchina, Angew. Chem. Int. Ed. 117 (2005) 4852–4855.
- [9] M.M. Fan, P.B. Zhang, Energy Fuels 21 (2007) 633–635.
- [10] R.X. Bai, Y. Wang, S. Wang, F.M. Mei, T. Li, G.X. Li, Fuel Process Technol. 106 (2013) 209–214.
- [11] Y.T. Kim, E.D. Park, Appl. Catal. A 356 (2009) 211–215.
- [12] D. Delle Donne, F. Rivetti, U. Romano, Appl. Catal. A 221 (2001) 241–251.
- [13] K.M. Su, Z.H. Li, B.W. Cheng, K. Liao, D.X. Shen, Y.F. Wang, J. Mol. Catal. A 315 (2010) 60–68.
- [14] H. Kominami, A. Tanaka, K. Hashimoto, Chem. Commun. 46 (2010) 1287–1289.
- [15] A. Tanaka, K. Hashimoto, H. Kominami, Chem. Commun. 47 (2011) 10446–10448.
- [16] S. Sarina, H.Y. Zhu, Z.F. Zheng, S. Bottle, J. Chang, X.B. Ke, J.-C. Zhao, Y.N. Huang, A. Sutrisno, M. Willans, G.R. Li, Chem. Sci. 3 (2012) 2138–2146.
- [17] P.R. Liu, H.M. Zhang, H.G. Liu, Y. Wang, X.D. Yao, G.S. Zhu, S.Q. Zhang, H.J. Zhao, J. Am. Chem. Soc. 133 (2011) 19032–19035.
- [18] G.H. Qina, Y. Zhang, X.B. Ke, X.L. Tong, Z. Sun, M. Liang, S. Xue, Appl. Catal. B 129 (2013) 599–605.
- [19] Z.F. Zheng, J. Teo, X. Chen, H.W. Liu, Y. Yuan, E.R. Waclawik, Z.Y. Zhong, H.Y. Zhu, Chem. Eur. J. 16 (2010) 1202–1211.
- [20] L.J. Liu, J. Chan, T.K. Sham, J. Phys. Chem. C 114 (2010) 21353–21359.
- [21] R.L. Penn, J.F. Banfield, Am. Mineral 84 (1999) 871–876.
- [22] D.J. Yang, H.W. Liu, Z.F. Zheng, Y. Yuan, J.C. Zhao, E.R. Waclawik, X.B. Ke, H.Y. Zhu, J. Am. Chem. Soc. 131 (2009) 17885–17893.
- [23] H.Y. Zhu, Y. Lan, X.P. Gao, S.P. Ringer, Z.F. Zheng, D.Y. Song, J.C. Zhao, J. Am. Chem. Soc. 127 (2005) 6730–6736.
- [24] O. Haba, I. Itakura, M. Ueda, S. Kuze, J. Polym. Sci. Part A: Polym. Chem. 37 (1999) 2087–2093.
- [25] M. Zhang, Q. Wang, C.C. Chen, L. Zang, W.H. Ma, J.C. Zhao, Angew. Chem. Int. Ed. 68 (2009) 6081–6084.
- [26] S. Higashimoto, N. Kitao, N. Yoshida, T. Sakura, M. Azuma, H. Ohue, Y. Sakata, J. Catal. 266 (2009) 279–285.
- [27] S. Kim, W. Choi, J. Phys. Chem. B 109 (2005) 5143–5149.

- [28] M.J. Hu, J.J. Xu, J.F. Gao, S.L. Yang, J.S.P. Wong, R.K.Y. Li, *Dalton Trans.* 42 (2013) 9777–9784.
- [29] X.H. Guan, G.H. Chen, C. Shang, *J. Environ. Sci.* 19 (2007) 438–443.
- [30] F. Ungureanu, L. Voicu, I. Andrei, *J. Optoelectron. Adv. Mater.* 8 (2006) 315–318.
- [31] D. Srinivas, R. Srivastava, P. Ratnasamy, *Catal. Today* 96 (2004) 127–133.
- [32] P.N. Gooden, R.A. Bourne, A.J. Parrott, H.S. Bevinakatti, D.J. Irvine, M. Poliakoff, *Org. Process Res. Dev.* 14 (2010) 411–416.
- [33] Y.X. Zhou, J.L. Song, S.G. Liang, S.Q. Hu, H.Z. Liu, T. Jiang, B.X. Han, *J. Mol. Catal. A* 308 (2009) 68–72.
- [34] H.G. Li, M. Vrinat, G. Berhault, D.D. Li, H. Nie, P. Afanasiev, *Mater. Res. Bull.* 48 (2013) 3374–3382.
- [35] F. Wang, W. Ueda, J. Xu, *Angew. Chem. Int. Ed.* 124 (2012) 3949–3953.
- [36] H. Bohets, B.J. van der Veken, *Phys. Chem. Chem. Phys.* 1 (1999) 1817–1826.
- [37] T. Hongo, A. Yamazaki, *Micropor. Mesopor. Mater.* 142 (2011) 316–321.